The impact of a future solar minimum on climate change projections in the Northern Hemisphere

2016 Environ. Res. Lett. 11 034015

(http://iopscience.iop.org/1748-9326/11/3/034015)

Environmental Research Letters

LETTER

The impact of a future solar minimum on climate change projections in the Northern Hemisphere

G Chiodo[1,8], R García-Herrera[1,2], N Calvo[1], J M Vaquero[3], J A Añel[4,5], D Barriopedro[1,2] and K Matthes[6,7]

[1] Dpto. Astrofísica y CC de la Atmosfera, Fac. de Ciencias Físicas, Universidad Complutense, Madrid, Spain
[2] Instituto de Geociencias (IGEO), Madrid, Spain
[3] Universidad de Extremadura, Mérida, Spain
[4] Smith School of Enterprise and the Environment, University of Oxford, Oxford, UK
[5] EPhysLab, Universidade de Vigo, Ourense, Spain
[6] GEOMAR Helmholtz Center for Ocean Research Kiel, Kiel, Germany
[7] Christian-Albrechts Universitaet zu Kiel, Kiel, Germany
[8] Current address: Department of Applied Physics and Applied Mathematics, Columbia University, New York (NY), USA.

E-mail: chiodo@columbia.edu

Keywords: climate change projections, global models, future solar minimum

Supplementary material for this article is available online

OPEN ACCESS

RECEIVED
19 February 2015

REVISED
17 February 2016

ACCEPTED FOR PUBLICATION
18 February 2016

PUBLISHED
7 March 2016

Abstract

Solar variability represents a source of uncertainty in the future forcings used in climate model simulations. Current knowledge indicates that a descent of solar activity into an extended minimum state is a possible scenario. With aid of experiments from a state-of-the-art Earth system model,we investigate the impact of a future solar minimum on Northern Hemisphere climate change projections. This scenario is constructed from recent 11 year solar-cycle minima of the solar spectral irradiance, and is therefore more conservative than the 'grand' minima employed in some previous modeling studies. Despite the small reduction in total solar irradiance (0.36 W m^{-2}), relatively large responses emerge in the winter Northern Hemisphere, with a reduction in regional-scale projected warming by up to 40%. To identify the origin of the enhanced regional signals, we assess the role of the different mechanisms by performing additional experiments forced only by irradiance changes at different wavelengths of the solar spectrum. We find that a reduction in visible irradiance drives changes in the stationary wave pattern of the North Pacific and sea–ice cover. A decrease in UV irradiance leads to smaller surface signals, although its regional effects are not negligible. These results point to a distinct but additive role of UV and visible irradiance in the Earth's climate, and stress the need to account for solar forcing as a source of uncertainty in regional scale projections.

1. Introduction

A number of studies have recently raised the possibility of a near-future descent of solar activity into a new grand minimum state, similar to the grand maunder minimum (Abreu *et al* 2008, Lockwood *et al* 2011, Roth and Joos 2013, Zolotova and Ponyavin 2014). The weakness of the current solar cycle number 24, and the unusually deep minimum in 2008–2009 (Janardhan *et al* 2011, Lockwood 2011, Nandy *et al* 2011) support this view. However, model projections of the 21st century participating in the Fifth Coupled Model Intercomparison Project (CMIP5) did not account for long-term changes in solar variability in the future, other than repeating the previous solar cycle number 23 or the last four observed solar cycles (Kirtman *et al* 2013, Myhre *et al* 2013). Thus, the solar forcing employed in CMIP5 model projections may not be representative of realistic future conditions. In this context, it is necessary to assess the potential impact of a hypothetical future solar minimum on climate change projections.

With this rationale, a number of studies have been performed with intermediate complexity (Feulner and Rahmstorf 2010), box-diffusion (Jones *et al* 2012), and fully coupled ocean–atmosphere models (Anet *et al* 2013, Meehl *et al* 2013, Ineson *et al* 2015, Maycock *et al* 2015). A range of future solar minimum scenarios

were employed, involving reductions in the total solar irradiance (TSI) of 0.4% (Anet *et al* 2013), 0.25% (Meehl *et al* 2013), 0.12% (Ineson *et al* 2015, Maycock *et al* 2015) and 0.08 % (Feulner and Rahmstorf 2010, Jones *et al* 2012). These studies were instructive in showing that even a 'grand' minimum state would only partly reduce (by 0.1 K), or delay the projected rise in global mean temperature (Anet *et al* 2013, Meehl *et al* 2013). More moderate scenarios would result in an even weaker signal (Feulner and Rahmstorf 2010, Jones *et al* 2012). While there is consensus on the small impact of a solar minimum on global warming, the effects on regional scales are still poorly understood.

More recently, it was shown that a future grand minimum would lead to a significant reduction in the projected warming tendency over Eurasia (Ineson *et al* 2015, Maycock *et al* 2015). These authors performed different solar perturbation experiments, one including a 0.12% reduction in TSI that was apportioned across the spectrum according to the CMIP5 recommendation, and one with a larger 0.85% reduction (-1.75 W m^{-2}) in the UV irradiance alone. They identify similar regional responses in the Northern hemisphere (NH) in both experiments, with a magnitude that does not appear to scale linearly with the forcing magnitude. Nevertheless, the forcing employed in their experiments, motivated by reconstructions of the maunder minimum, was larger than that observed over the 11 year solar cycle.

It has been shown that the accuracy of solar proxy data back to the maunder minimum is limited (Solanki and Fligge 1999). Moreover, the new sunspot reconstructions indicate that, in contrast to older versions, there was a very small but detectable 11 year solar cycle during the maunder minimum (Usoskin *et al* 2015). Thus, previous sunspot-based reconstructions of solar forcing were possibly overestimating the amplitude of the TSI decrease during the maunder minimum relative to present-day. In this context, it has recently been suggested that the solar minimum in 2008–2009 could better represent the actual TSI values for the maunder minimum (Schrijver *et al* 2011). Therefore, a feasible future scenario of solar activity may involve a decrease in 11 year variability, with smaller TSI changes than those considered in some recent modeling studies.

A future decrease in the 11 year solar cycle variability could be predominantly driven by changes in certain spectral regions, such as visible and UV, as supported by current observational estimates of solar spectral irradiance (SSI) forcing (Ermolli *et al* 2013). Instead, previous studies employed a spectrally uniform decrease in SSI (Feulner and Rahmstorf 2010, Jones *et al* 2012). Some studies imposed a wavelength-dependent decrease throughout the spectrum (thus in both UV and visible wavelengths), consistent with the forcing modeled by Lean *et al* (2005) (e.g., Anet *et al* 2013, Meehl *et al* 2013). More recently, the impact of TSI and UV forcings was also investigated (Ineson *et al* 2015, Maycock *et al* 2015). These papers give insights into the role of the UV-driven top-down mechanism on Northern Hemispheric climate change in the second half of the 21st century (2050–2099) in an extreme GHGs scenario (i.e., the RCP8.5). However, the use of different magnitudes for TSI and UV forcings in their simulations makes it difficult to accurately assess the relative contribution of visible and UV wavelengths to the model response to a given TSI perturbation. Thus, disentangling the top-down and visible-driven bottom-up feedbacks (see e.g., Meehl *et al* 2009) in the full response to SSI changes is an unsolved issue, which is of crucial relevance to understand the influence of solar activity on Earth's climate, and its potential role in modulating future climate change signals on regional scales.

In this paper, we explore the impact of a solar minimum scenario on 21st century climate change projections (2005–2065), which is calculated as a mean of the SSI over the minima recorded in the last four 11 yr solar cycles. This type of forcing is novel and better constrained than previous estimates in that it is constructed from SSI values from recent solar cycle minima, and not from reconstructions of the maunder minimum. In contrast to other modeling studies also imposing a conservative minimum scenario (Feulner and Rahmstorf 2010, Jones *et al* 2012), we further consider a spectrally resolved solar forcing, and use a state-of-the-art Earth system model with interactive ozone chemistry. Furthermore, we carefully decompose the response due to the different wavelengths (visible versus UV), thereby identifying the feedbacks that enhance the sensitivity of regional-scale projections to solar irradiance.

2. Model description and simulations

We use the community Earth system model (CESM) version 1.0.5 (Marsh *et al* 2013), which includes the atmospheric component from the whole atmosphere community climate model version 4 (WACCM4), and the parallel Ocean program full ocean model. The atmospheric resolution is 1.9° latitude and 2.5° longitude with 66 vertical levels providing a well-resolved middle atmosphere and an upper boundary at 140 km. The atmosphere component WACCM4 is fully coupled with chemistry and radiation schemes. The CAMRT solar radiation module divides incoming shortwave radiation into 19 intervals from 200 to 5000 nm, seven of which are centered in the UV (200–350 nm) and two in the visible (350–700 nm) range. The photochemistry scheme is based on MOZART-3 (Kinnison *et al* 2007), and has a resolution of 66 bands, covering all absorption lines from 120 nm onwards. Most importantly, the solar forcing is treated in a self-consistent way in the calculation of

heating and photolysis rates, as both radiation and chemistry modules use the same SSI flux.

We perform two ensembles of three members each over the 2005–2065 period. In both ensembles, the atmospheric loadings of well-mixed greenhouse gases (GHGs) and ozone depleting substances follow the representative concentration pathway 4.5 (RCP4.5), i.e., a mid-range scenario used in the IPCC-AR5 (Myhre *et al* 2013). In one ensemble, a transient 11 yr solar cycle is imposed by repeating the last four solar cycles (20–23) (red line in figure S1). Spectrally resolved irradiance data are taken from http://solarisheppa.geomar.de/cmip5. This ensemble, which is referred throughout the paper as RCP45, was previously used for the IPCC-AR5, and provides a reference case of climate change projections for the 21st century.

The second ensemble is driven with the same RCP4.5 forcings, except for solar activity, which is kept at constant SSI levels throughout a 58 year period, starting from the year 2008, as a continuation to the minimum of solar cycle number 23 (black line in figure S1). This ensemble is referred as MIN, since the SSI input is obtained by averaging it over the recorded years of solar minimum (1964, 1965, 1975, 1976, 1985, 1986, 1995, 1996, 2007, 2008), as derived from Lean *et al* (2005). The averages were calculated separately for each spectral band. More specifically, seven intervals were chosen for UV (200–245, 245–265, 265–275, 275–285, 285–294, 295, 305–350 nm) and two for the visible (350–640, 640–700 nm) irradiance, consistent with the bands of the CAMRT solar radiation scheme. On average over the simulated period, the MIN forcing implies a TSI reduction of 0.36 W m^{-2} (or 0.03%) relative to the RCP45 case, with an irradiance decrease in all wavelengths (i.e., both in visible and UV), although the magnitude of the decrease is spectrally dependent (i.e., 10% in the 200–245 nm band, tapering off to 0.03% in the 640–700 nm band).

In addition, two single experiments are performed to identify the mechanisms that contribute to the surface response to the imposed solar minimum. In these simulations, the solar minimum forcing is imposed separately in either the seven UV (200–350 nm) or two visible (350–700 nm) bands, respectively, while the rest of the spectrum contains the same sequence of 11 yr solar cycles prescribed in the RCP45 ensemble. As in the MIN forcing, the same SSI input is used for both radiation and photochemistry. Hence, changes in stratospheric ozone (brought about by changes in photolysis and heating rates) are calculated interactively. This represents a novelty over other studies exploring the regional effects of a spectrally resolved grand minimum forcing, which externally imposed an ozone forcing (Ineson *et al* 2015, Maycock *et al* 2015).

Due to the presence of a transient 11 year solar cycle in selected portions of the spectrum, the MINuv and MINvis forcings lead to a solar cycle in TSI, which is weaker than in the reference RCP45 case (see figure S1), with an average TSI decrease of 0.09 W m^{-2} and 0.27 W m^{-2}, respectively. The radiative forcing in MINuv strongly affects the stratosphere due to ozone absorption of UV radiation. Thus, any tropospheric and surface impact would be linked to a transmission of the solar signal from the stratosphere via the top-down stratospheric mechanism (see e.g., Haigh 1996, Shindell *et al* 1999, Kodera and Kuroda 2002). In the MINvis experiment, the decrease in the visible irradiance directly affects the surface radiation budget, thus isolating the component of the response associated with a direct impact of the solar forcing at the surface (Gray *et al* 2010).

In certain aspects, such as the numerical model employed and the set-up of RCP45 and MIN experiments, our work is similar to Meehl *et al* (2013). However, the key difference lies in the amplitude and duration of the solar dimming relative to the reference RCP45 case. In the present work, the forcing is consistent with present-day SSI levels recorded during minima of the sunspot cycle. This represents an SSI reduction eight times smaller than the −0.25% forcing imposed in Meehl *et al* (2013) who found a noticeable global mean response (see their figure1). Thus, the comparison of these experiments with those reported in Meehl *et al* (2013) gives insight into the linearity of the model response to solar forcing. In addition, the design of the idealized MINuv and MINvis experiments allows for unambiguous identification of processes leading to the full response at regional scale by their mutual interactions.

The MIN and RCP45 ensembles consist of three members each, making a total sample size of 183 years for each case. The influence of the solar minimum in future projections is quantified as the difference between the climatological mean of the idealized simulations and that of the reference RCP45 ensemble. Statistically significant differences are evaluated using a Student t-test, including a correction to take serial correlation into account (Zwiers and von Storch 1995). The null hypothesis is that the difference between the climatological averages of MIN and RCP45 ensembles is not significantly different from zero. Throughout the paper, differences are considered significant when they exceed the 0.05 significance (95% one-tail confidence) level.

3. Impact of solar minimum on climate change projections

In agreement with previous studies employing a moderate TSI reduction (Feulner and Rahmstorf 2010, Jones *et al* 2012), the impact of the solar minimum on the projections of global mean temperature obtained here is negligible, which is not surprising considering the small amplitude of the MIN forcing compared to the GHGs forcing. More specifically, a global mean temperature rise of approximately 0.2 K per decade is

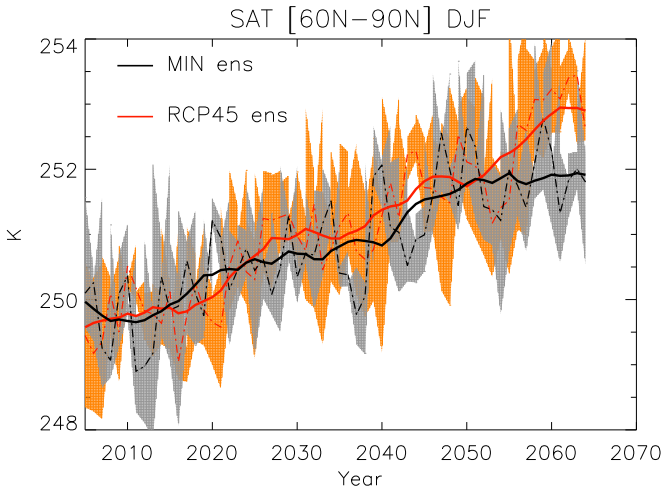

Figure 1. Time series of the surface air temperature (SAT) in boreal winter (DJF) averaged over NH high latitudes (60°N–90°N). The stippled lines indicate the winter mean ensemble average in the MIN (black) and RCP45 (red) simulations. The shading depicts the spread spanned by the three members of each ensemble, and is shown in gray and orange for the MIN and RCP45 ensembles, respectively. The bold lines indicate the running mean obtained with a 10 yr boxcar average. Units K.

found over the simulated period of both MIN and RCP45 simulations (not shown). Nevertheless, significant differences between the MIN and RCP45 ensembles arise in the NH high latitudes (60°N–90°N) in the December-to-February (DJF) mean (figure 1). In this region, the RCP45 warming trend is much larger than in the global mean, a behavior that is robust across all IPCC-AR5 models, and is commonly referred to as 'Arctic amplification' (Kirtman *et al* 2013) (see also figure S2(a)). Interestingly, the MIN forcing reduces the predicted high-latitude warming by ~1 K at the end of the simulated period, suggesting a reduction of the Arctic amplification.

To show this, we explore the spatial distribution of the boreal winter surface air temperature (SAT) response to MIN in the NH, computed as the difference between the 2005–2065 climatologies of the MIN and RCP45 ensemble means (figure 2(a)). A widespread cooling region is found over some parts of the Arctic, with peaks of 1.2 K in the Bering Sea. This response encompasses the eastern part of the Pacific basin at high latitudes, and extends to the western Tropical Pacific, representing a horse-shoe pattern, which resembles a negative phase of the Pacific decadal oscillation (PDO) (Mantua *et al* 1997). In the MIN ensemble, there is also significant cooling over Russia of up to 0.8 K, and warming of similar amplitude over eastern North America, and off the coast of Japan. To explore the relative impact of the MIN forcing on the climate change predictions, we compute the ratio of the local surface temperature change in the MIN ensemble to that of the RCP45, which is shown in figure S2(b). Locally, a 30%–40% change in the amplitude of the GHG-induced warming is evident in the aforementioned regions, indicating that in the WACCM model, a future solar minimum, similar to that of recent 11 yr solar cycle minima, alters the projected regional-scale warming in the NH.

The cooling signals at high latitudes are broadly similar in magnitude, although spatially more limited, to those reported by Anet *et al* (2013) (their figure S3), despite the larger TSI reduction employed in their study. Qualitatively similar surface responses were also found for different types of SSI forcing by Ineson *et al* (2015) and Maycock *et al* (2015), although the spatial distribution of the response is different, which is possibly due to the consideration of a different period (2005–2065 versus 2050–2099), GHG scenario (RCP4.5 versus RCP8.5) and UV forcing amplitude. A similar cooling response, albeit spatially more uniform over the Arctic, was also reported in Meehl *et al* (2013) using the same model and GHGs scenario, but a much larger solar forcing than in the present work. Interestingly, the cooling signals over Russia and Alaska found here are of very similar magnitude to those obtained at the late stage of the simulations performed by Meehl *et al* (2013) (see their figure 3(c)), even when the global responses are very different. This indicates that, while the global response depends on the magnitude of the solar forcing change, the sensitivity at regional scales is larger and does not scale with the magnitude of the solar forcing. Thus, significant regional responses can be triggered by small changes in the solar forcing.

The agreement between the present results and previous studies employing a larger minimum forcing suggests that the high northern latitudes are particularly sensitive to solar forcing, pointing to the possible role of feedbacks in amplifying the boreal winter regional-scale response. Another possibility is that the differences seen in figure 2(a) are partially influenced by internal variability (Deser *et al* 2012), although this effect should be minimized in the ensemble mean. To confirm the robustness of the forced responses, we

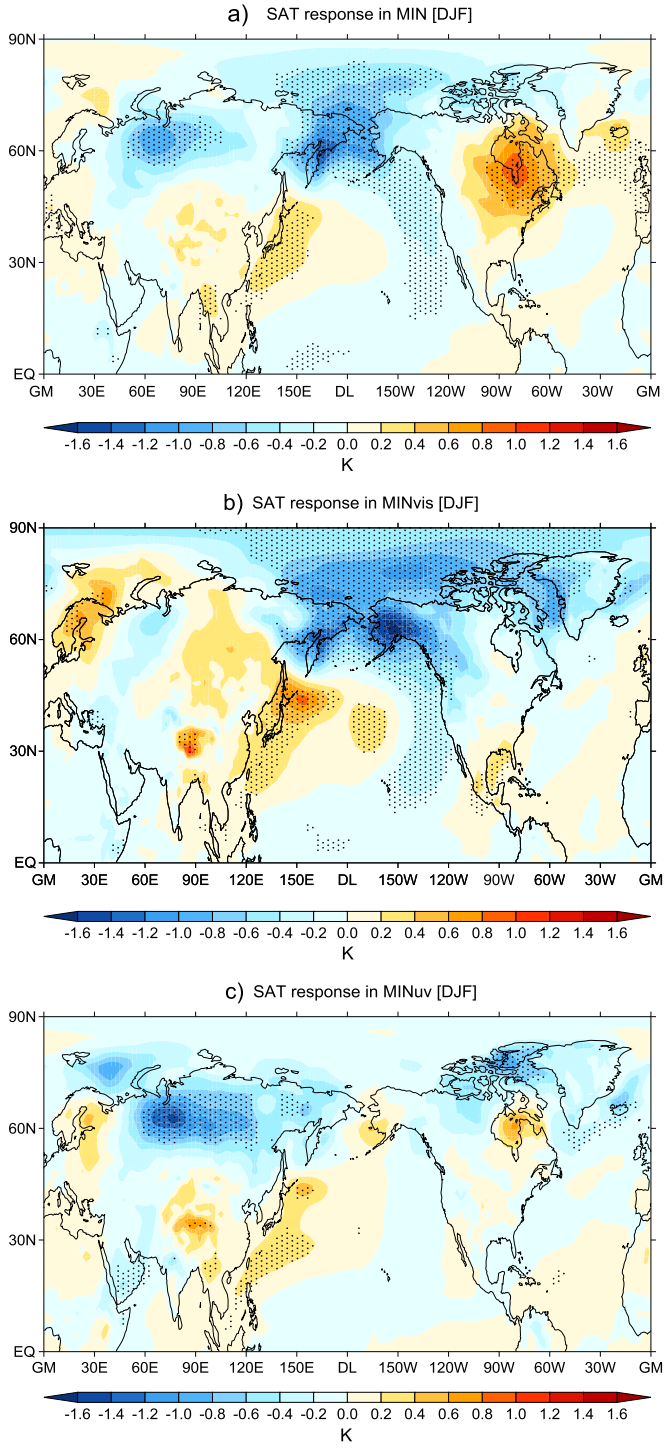

Figure 2. Northern Hemispheric boreal winter (DJF) SAT response, calculated as the difference over the simulated period (2005–2065) between (a) MIN minus RCP45 ensemble means, (b) MINvis minus RCP45, (c) MINuv minus RCP45. Stippled areas indicate significant differences at 95% confidence level. Contours are drawn every 0.2 K. Units K.

have performed the idealized MINuv and MINvis experiments, which further allow to isolate the role of top-down and bottom-up feedbacks.

The cooling in the Bering sea and the PDO-like structure extending to the western Tropical Pacific (Warm Pool region) are reproduced in the MINvis simulation (figure 2(b)), which indicates that part of the Pacific response to MIN is driven by direct changes in the radiative balance at the surface through the dimming in visible irradiance. On the other hand, the signal over Russia is well captured in the MINuv experiment (figure 2(c)), which points to a possible contribution of the ozone-mediated top-down mechanism in the surface response to MIN (see e.g., Haigh 1996, Matthes *et al* 2006, Gray *et al* 2010, Ineson *et al* 2015). Interestingly, the warming over eastern

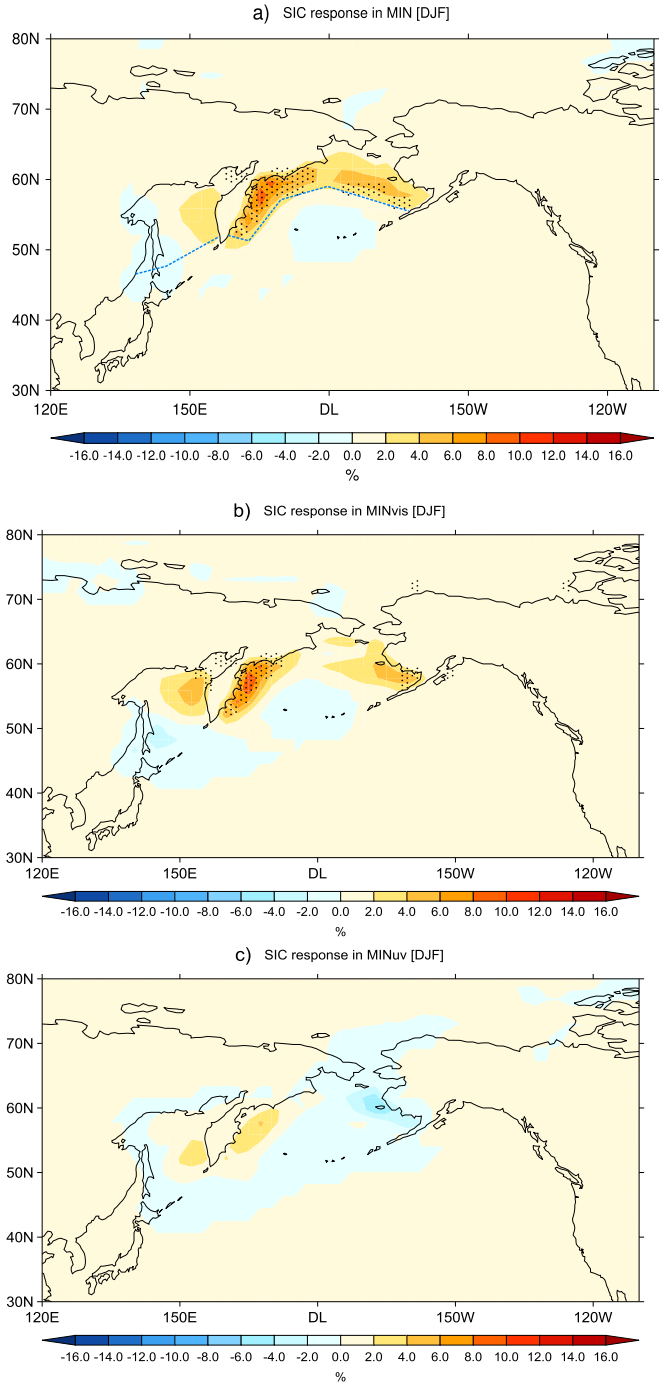

Figure 3. As in figure 2, but for the sea ice concentrations (SIC) response in the NH Pacific sector. The sea–ice edge simulated in the RCP45 ensemble during the 2005–2015 period is represented by the blue stippled line (estimated as the lowermost grid cell containing more than 30% of sea–ice). Contours are drawn every 2 units, corresponding to a 2% change in winter mean SIC.

North America is partly reproduced in the MINuv experiment, although it is weak and not statistically significant, indicating that this feature more likely involves an interaction of both UV and visibile forcings.

Taken together, the results from the idealized experiments rule out a role of internal variability in producing the regional-scale differences in the projected warming in the NH. Thus, in the following sections we explore the mechanisms associated with the visible and UV-driven feedbacks.

3.1. Contribution of the bottom-up mechanism

Motivated by the important role of the cryosphere in the projected Arctic amplification (Holland and Bitz 2003, Serreze *et al* 2009, Serreze and Barry 2011), we first explore sea–ice changes. Figure 3(a) shows the simulated boreal winter mean sea–ice concentration (SIC) response to MIN in the Bering strait. Relative to the RCP45 ensemble, the MIN ensemble shows a SIC increase of 8% in the coastal regions of Alaska and Russia, which is where the sea–ice edge is located during the first simulated decade (2005–2015). This is

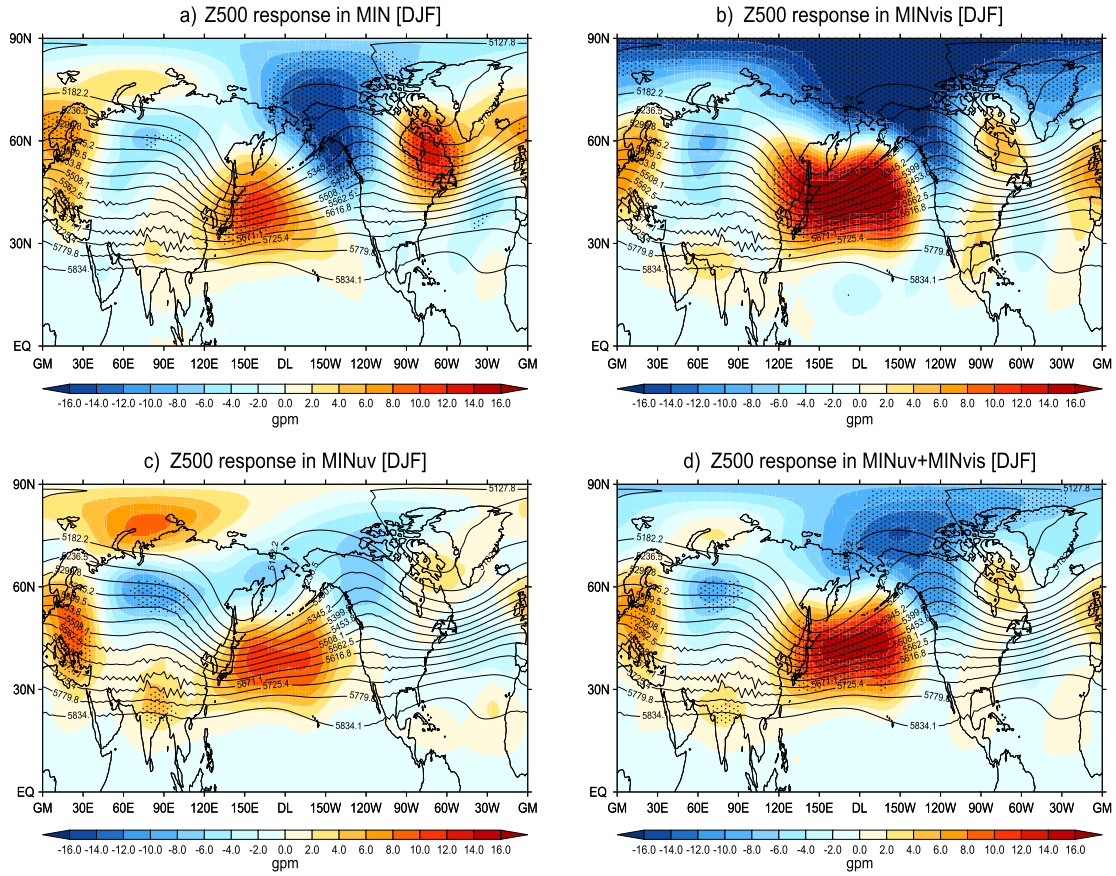

Figure 4. As in figure 2, but for the difference of 500 hPa Geopotential Height between (a) MIN minus RCP45 ensemble, (b) MINvis minus RCP45, (c) MINuv minus RCP45, and (d) MINuv+MINvis minus RCP45. Shading contours are drawn every 2 gpm. Black contour lines represent the climatological values in the RCP45 ensemble. Units gpm.

partly reproduced in the MINvis experiment (figure 3(b)), while the UV forcing does not lead to any significant SIC changes (figure 3(c)). The SIC increase enhances the localized cooling over Alaska (figure 2(a)) through an increase in surface albedo, and a reduction in heat flux exchange between ocean and the overlying atmosphere. Increased coastal SIC is supported by westerly wind anomalies over the Bering strait in MIN and MINvis, as they induce southward sea–ice export from the Bering strait, and the onset of cooler SSTs in the eastern Pacific. A similar sea–ice effect was also argued to amplify the effects of a solar minimum under a global warming scenario, as compared to preindustrial conditions (Song *et al* 2010). However, Song *et al* (2010) applied a much stronger and spectrally uniform irradiance decrease in their simulations of 2.7 W m^{-2}, which is one order of magnitude larger than the irradiance reduction employed here.

The magnitude and extent of the regional surface signals seen in figure 2(a) are arguably too large to be solely explained by changes in SIC. Therefore, we also explore changes in atmospheric circulation. These can be investigated by analyzing changes in geopotential at 500 hPa, which are displayed in figure 4 for MIN (panel (a)), MINvis (panel (b)) and MINuv (panel (c)). As compared to RCP45, the MIN ensemble shows a weakened stationary wave pattern, as evidenced by anomalous ridges off the coast of Japan and eastern North America, and a trough anomaly over Alaska. A similar pattern is found in sea-level pressure (SLP) (not shown), which suggests that the circulation response to the MIN forcing is, to a certain degree, barotropic. The dipole of geopotential anomalies are (geostrophically) consistent with the temperature patterns shown in figure 2(a). First, the anomalous ridges over the Hudson Bay and the western Pacific produce more southerly flow, and therefore positive surface temperature anomalies over eastern North America and off the coast of Japan. Second, the weakened ridge in the eastern Pacific is linked to an increase in the meridional SLP gradient and stronger surface westerlies in the Aleutian sector, which result in increased southeastward transport of cooler surface water and a negative sea surface temperature (SST) anomaly in this region (see e.g., Hartmann 1994), in agreement with the horse-shoe cooling pattern observed in figure 2, and the increase in sea–ice (figure 3).

The anomalies in the Pacific sector are partly reproduced in MINvis (figure 4(b)). There is also a similar response in the MINuv integration (figure 4(c)), although it is weaker and not significant,

indicating that most of the circulation response in this region is driven by the visible irradiance forcing, involving a bottom-up mechanism. We note that the weakening of the Alaska ridge in the Pacific in the MIN ensemble (figure 4(a)) is qualitatively consistent with the observed deepening of the Aleutian Low during 11 year solar minima (van Loon *et al* 2007, Roy and Haigh 2010). Therefore, even though the forcing imposed in MIN is fundamentally different from a transient 11 year cycle, the circulation response in the NH is similar. Imposing a solar forcing change over a multi-decadal period leads to basin scale circulation patterns resembling decadal scale modes in the Pacific, such as the PDO, which is in agreement with the results obtained by Ineson *et al* (2015), Maycock *et al* (2015) using a larger minimum forcing. In this context, previous studies reported a dependence of the 11 year solar cycle signal in geopotential on the phase of the PDO (van Loon and Meehl 2014). However, in our simulations there is no evidence of a modulation of the MIN response pattern by the PDO phase itself (not shown), which rules out a role of internal variability in the tropospheric circulation response to the MIN forcing.

Comparing the geopotential response with the eddy barotropic streamfunction at upper tropospheric levels (300 hPa), it is possible to infer the portion of the circulation response that is coherent with changes in stationary Rossby waves (see e.g., Held *et al* 2002). These are shown in figure 5 for the MIN (a), MINvis (b) and MINuv (c) experiment. In the MIN ensemble, one Rossby wave train (RWT) emanating from the tropical Pacific can be identified, and is shown by the stippled black line. Its approximate ray path propagates northward, and is subsequently deflected equatorward in the Atlantic sector.

There is good resemblance between the geopotential and streamfunction anomalies (compare figures 4(a) and 5(a)), which indicates that the extratropical circulation response in the MIN experiment is coherent with a RWT generated in the tropics. A similar RWT is reproduced in MINvis (figure 5(b)) and MINuv (figure 5(c)), although the anomalies in RWT and consequently in geopotential are only significant in the former case, consistent with the dominant role of the visible irradiance forcing changes in driving the MIN response. None of these idealized experiments captures the full amplitude and downstream extent of the MIN ensemble wave pattern, which explains the weaker geopotential and temperature response over the Hudson bay in these integrations.

One possible triggering mechanism for RWTs is convective heating (Simmons 1982, Jin and Hoskins 1995), which can be calculated in WACCM as the vertically integrated temperature tendency produced by the convective parameterization. The projected changes in this quantity are shown in figure S3. Relative to the RCP45 ensemble, the MIN ensemble (figure S3(a)) shows a decrease in the convective heating over the Warm Pool region, and consequently, in tropical precipitation (not shown). Again, a similar response is reproduced in MINvis (figure S3(b)), which suggests that the suppressed convective activity in MIN is mainly driven by reduced visible irradiance. Note that the weak convection is linked to cooling in the central-eastern subtropical Pacific and Warm Pool region (see figure 2), and smaller moisture availability due to suppressed latent heat flux (which decreases on average over these regions by 1.25 W m^{-2}), consistent with the solar cycle response in the tropical Pacific (Meehl *et al* 2003, Meehl and Arblaster 2009). As the coupling between deep convection and surface energy fluxes is strongest in regions where SSTs >27 °C (Zhang 1993), the response in convective activity to surface temperature changes is confined to the Warm Pool region. This western Pacific anomaly induces convergence at upper tropospheric levels (see figure S4) and a cyclonic vorticity perturbation, triggering the RWT in the MIN and MINvis (figure 5).

Note that the tropical Pacific response to a future solar minimum is consistent with the bottom-up mechanism formulated in Meehl *et al* (2009) in that a reduction in visible irradiance and the consequent circulation feedbacks lead to a weakening of climatological precipitation maxima, such as the Warm Pool region. The presence of a persistent solar forcing in the MIN ensembles allows the diabatic heating response to influence the circulation of the NH, thus extending the impact of the bottom-up feedbacks to the NH high latitudes. However, the response in the eastern tropical Pacific region does not resemble an El-Niño pattern (see figure 2), in contrast to what would be expected for 11 year solar minimum conditions according to Meehl and Arblaster (2009), Meehl *et al* (2009). This indicates that the long-term Pacific response does not project onto a warm ENSO mode, consistent with the weak eastern Pacific response obtained in Meehl *et al* (2013) (see their figure 3(c)).

To confirm that the diabatic heating change shown in figure S3 is a forcing rather than a feedback of the circulation changes observed in the Pacific, we performed simulations with a nonlinear stationary wave model, which is described in detail in Ting and Yu (1998). This model allows diabatic heating and circulation responses to be separated in a causal way. Due to this unique feature, it has been employed in a number of recent studies on the tropospheric circulation response to zonally asymmetric forcings (Kushnir *et al* 2010, Seager *et al* 2010, Simpson *et al* 2015).

We forced the model using a similar set-up as in Simpson *et al* (2015), but adding a diabatic heating perturbation of -0.5 K d^{-1} over the Warm Pool region, which mimics the heating anomaly simulated in WACCM (figure S3(a)). The transient eddy streamfunction response at 300 hPa is shown in figure S5 in a sequence running from day 1–3 (figure S5(a)), to day 13–16 (figure S5(e)). After day 1–3, the wave train is refracted eastward due to the presence of the

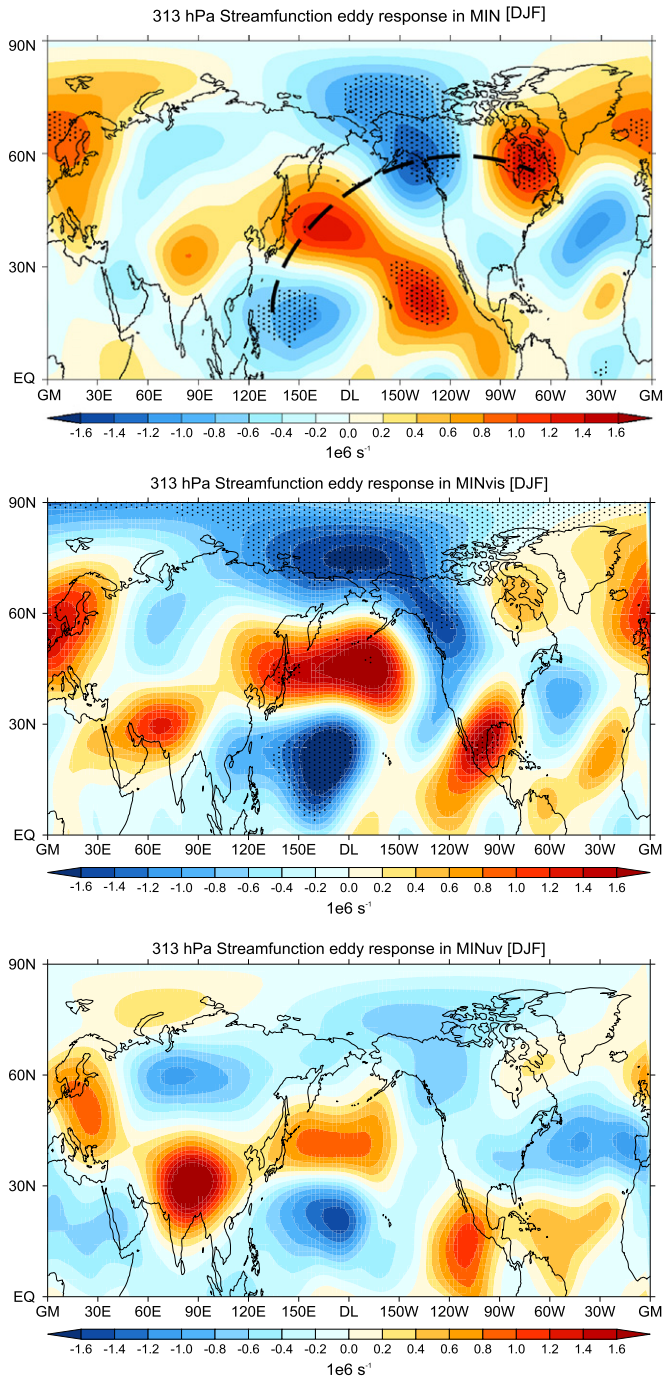

Figure 5. As in figure 2, but for upper tropospheric (313 hPa) eddy streamfunction. Contours are drawn every 0.2 $\times$ 10^6 s^{-1}. The black stippled line in figure 5(a) is drawn by connecting successive troughs/ridges, and it represents the approximate ray path of a Rossby-wave train simulated in the idealized stationary wave model (see figure S5). Units s^{-1}.

mid-latitude jet, which acts to decrease the stationary wavenumber (see e.g., Hoskins and Ambrizzi 1993). The response after day 16 is very similar to the 13–16 d average (figure S5(e)), which indicates that a steady-state has been reached (not shown). The main features of the North Pacific response in WACCM are qualitatively reproduced, albeit with some discrepancies over the Asian continent (compare figure S5(e) and 5(a)). More specifically, the northward–eastward propagation of the wave front in the idealized model is very similar to the RWT simulated by WACCM (figure 5(a)), thus indicating its adequacy in describing, at least qualitatively, the approximate trajectory taken by the RWT in the MIN ensemble. These results confirm that the MIN circulation responses over the Pacific are forced by diabatic heating anomalies in the Warm Pool region, which are in turn mainly driven by visible irradiance changes. Interestingly, the amplitude of the dipole over Alaska and North America simulated by the idealized model is much smaller than in WACCM, suggesting that additional sources neglected in this model are instrumental in amplifying the RWT

in the North Pacific. These may include changes in baroclinicity induced by the sea–ice response at surface levels (figure 3) (e.g., Overland and Wang 2010, Bader *et al* 2011) and transient eddy vorticity fluxes (e.g., Harnik *et al* 2010).

According to these results, the surface temperature signal in the Pacific basin for the MIN experiments (figure 2(a)) is due to a combination of circulation and sea–ice feedbacks. Contributions from these feedbacks amplify regional scale solar effects in regions where the sea–ice edges progressively shrink due to global warming, such as the Bering Strait, and also in other extratropical regions via RWT-induced responses forced by tropical convection changes. The effects of the UV forcing in the MIN Pacific response seem to be of secondary importance, although they may interact with the signal associated with visible irradiance.

Insights into the additivity of the circulation response to the MIN forcing in WACCM can be gained by adding the 500 hPa geopotential responses from both idealized experiments (MINuv + MINvis), which is shown in figure 4(d). The decrease in geopotential over Russia and Alaska, and the positive anomaly in the Pacific seen in MIN (figure 4(a)) are qualitatively well reproduced by the linear superposition of the individual UV and visible forced responses, indicating that the effects of UV and visible are, to a certain degree, additive. On the other hand, the dipole of negative and positive geopotential anomalies over Alaska and the Hudson Bay is underestimated, indicating that visible and UV effects on circulation are amplified when they vary together/at the same time (i.e., in the MIN ensemble) resulting in a regional amplification of the warming tendency relative to the RCP45 case (figure S2).

3.2. Contribution of the top-down mechanism

While circulation and sea–ice feedbacks induced by changes in visible irradiance are the main drivers of the MIN response, they do not explain the cooling simulated over Russia seen in figure 2. This pattern appears intensified in the first half of the simulation (2005–2035), when the MIN and MINuv responses are characterized by an SLP increase over Russia and part of the Arctic. Anomalous high pressure at these latitudes in winter leads to an increase of radiative cooling at surface levels, and thus fosters the development of cold anomalies. Together with the positive SLP anomalies over the polar cap (not shown), the hemispheric pattern is reminiscent of a negative phase of the Arctic oscillation (AO) (Thompson and Wallace 1998), and one of the clearest manifestations of stratosphere-troposphere dynamical coupling.

One possible pathway to explain the projection onto the AO mode is through changes in the tropical lower stratosphere, which can trigger synpotic eddy feedbacks in the mid-latitude tropopause region (Haigh *et al* 2005, Simpson *et al* 2009). However, there is no evidence of significant tropical lower stratospheric temperature changes in the MIN ensemble (not shown), which indicates that this mechanism plays little role in the surface response seen in figure 2.

Another possible pathway for the top-down solar mechanism is through changes in the stratospheric polar vortex (e.g., Kodera and Kuroda 2002). To investigate this mechanism, the cross-section of the zonal mean zonal wind response to the MIN forcings over the same period (2005–2035) is analyzed (figure 6(a)). Significant easterly anomalies are simulated in the NH high latitudes in the MIN experiment, reaching 2.5 m s^{-1} at 30–40 km, and extending to the lower troposphere and surface at 60–70°N. These signals reflect a weakening of the stratospheric polar vortex, in connection with the weakening of the zonal mean flow in the troposphere. The weakening in polar stratospheric westerly winds is caused by a decrease in UV absorption by ozone at low latitudes, whereby the meridional temperature gradient decreases (not shown).

In the lower stratospheric-upper tropospheric region, the weakening of westerly winds is partly reproduced in the MINuv experiment (figure 6(c)), indicating that the surface signal over Russia in MIN could be partly linked to a stratospheric top-down mechanism. This is also supported by previous studies reporting a cooling over Siberia in solar minimum scenarios driven by larger changes in UV irradiance (Anet *et al* 2013, Ineson *et al* 2015, Maycock *et al* 2015). Nevertheless, the MINuv response at 40 km (i.e., the core of the stratospheric jet) does not resemble the MIN response. In addition, the weakening of the stratospheric polar vortex and the positive SLP responses over Russia are not reproduced over the entire simulated period (2005–2065). This possibly occurs because in the second half of the simulated period (2035–2065), the stratospheric signal induced by the UV forcing is obscured by internal variability of the polar vortex, as indicated by the more frequent occurrence of sudden stratospheric warmings over this period in the RCP45 ensemble, which increased from 0.41 events/year in 2005–2035 to 0.56 events/year in 2035-2065. We argue that the lack of a robust stratospheric response (and consequently of the top-down contribution to surface signals) is due to the weak UV irradiance decrease relative to the RCP45 ensemble, which is half the magnitude of an 11 year solar cycle. In favor of this explanation, the sensitivity study performed by Maycock *et al* (2015) indicates that a more robust top-down propagation of the signal is reproduced if the UV forcing is increased by a factor of 5 (compare their figures 8(a) and 13(a)). These results suggest that the top-down contribution to surface signals largely depends on the amplitude of the UV forcing. A more detailed analysis involving simulations with different levels of UV forcing would be needed to elucidate this, which is beyond the scope of this paper.

Taken together, these results indicate that the influence of the UV-driven top-down mechanism is smaller

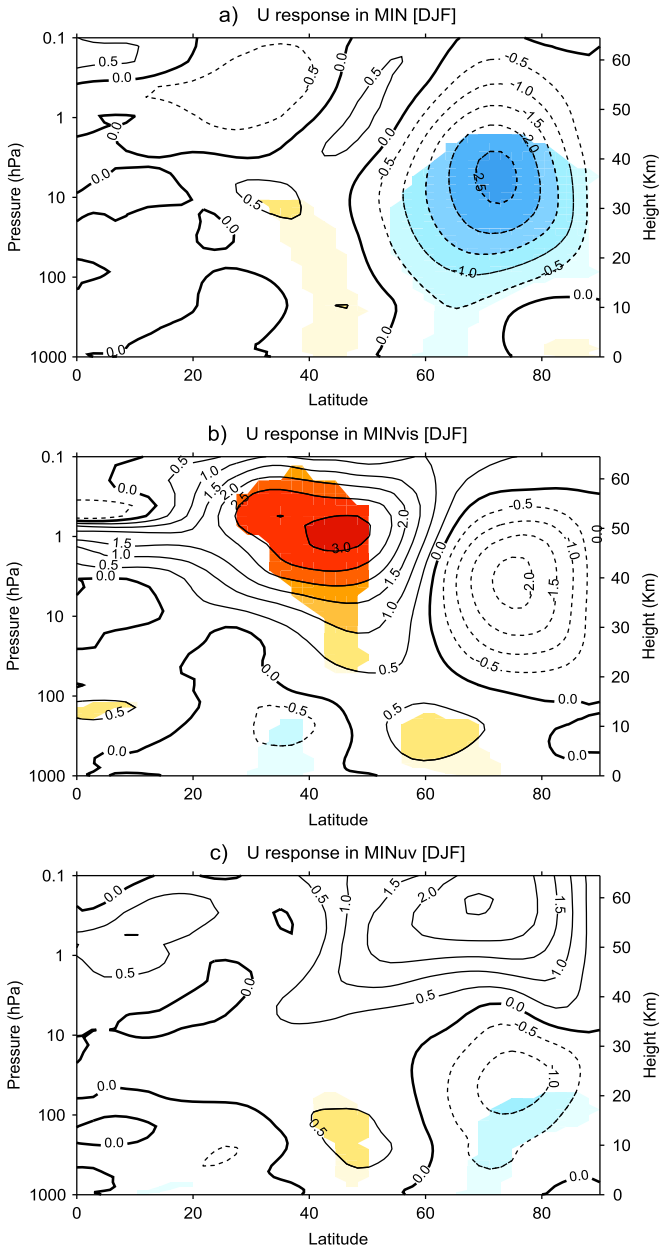

Figure 6. As in figure 2, but for the latitude-height cross-section of the zonal mean zonal wind response in the first half of the simulated period (2005–2035). Colous highlight regions where differences are statistically significant at 95% confidence level. Contours are drawn every 0.5 ms^{-1}. Units ms^{-1}.

in amplitude than the visible-driven circulation changes discussed in the previous section, likely due to the small UV forcing used in these simulations. In spite of this, the contribution of the UV is non-negligible, by either determining much of the total MIN response in some regions, such as over Russia, or by modulating it by enhancing the response associated with visible irradiance, such as in the Hudson Bay region.

4. Conclusions

As pointed out in earlier studies, the inability to predict the long-term evolution of solar activity is a source of uncertainty in future climate projections. Here, we quantify the impact of a solar minimum forcing in future projections by using an ensemble of simulations with a state-of-the-art climate model. The solar minimum forcing employed in this paper is close to present levels, albeit with an inhibited 11 yr cycle, following what recent evidences have proposed for the future (Schrijver *et al* 2011, McCracken and Beer 2014, Zolotova and Ponyavin 2014). In this sense, our scenario is more plausible than others because spectral irradiance changes are obtained from the recent solar cycle minima, rather than imposing irradiance values based on reconstructions of the maunder minimum (Lean 2000, Shapiro *et al* 2011).

In agreement with other models using a similarly moderate minimum scenario (Feulner and Rahmstorf 2010, Jones *et al* 2012), we do not find a

hemispheric-wide reduction in the GHG-driven warming. The lack of a uniform cooling response is due to the small irradiance reduction employed in the simulations, as compared to results obtained from more extreme minimum scenarios (Anet *et al* 2013, Meehl *et al* 2013, Ineson *et al* 2015, Maycock *et al* 2015).

While this scenario of reduced 11 year solar variability is predicted to have a negligible influence on the global warming tendency in the future, our results suggest a substantial modulation of regional scale warming patterns over the NH continental regions during winter. The spatial pattern is similar to that reported in Meehl *et al* (2013) using the same model, but much larger solar minimum forcing, which suggests that in WACCM, the high latitude regional responses in the NH do not scale linearly with the forcing. This is consistent with evidence from other models (Ineson *et al* 2015, Maycock *et al* 2015), indicating that a descent of solar activity into a shallow or deep minimum could result in similar regional climate effects in the NH.

Unlike previous studies, we also explore these regional responses and the involved mechanisms by performing additional model simulations to separate and quantify the relative contributions arising from changes in the visible and UV irradiances. The response to the solar minimum is linked to a bottom-up mechanism involving reduced convection in the equatorial Pacific, the generation of a RWT to the extratropics, and sea–ice changes, which are primarily driven by visible irradiance.

Overall, the influence of UV irradiance is smaller, although it leads to significant cooling over Russia. The little role played by the UV forcing is in contrast with evidence from other models (Ineson *et al* 2015, Maycock *et al* 2015). We argue that this apparent discrepancy is due to the relatively small UV forcing employed in our model integrations, and the role of polar stratospheric variability in masking the signal. Thus, the contribution of the UV driven top-down signal might be more relevant in deeper solar minimum scenarios. In addition, the relative roles of UV and visible irradiance in driving circulation changes in the North Pacific may depend on the GHGs emission scenario and period considered in the analysis, which is due to the dependence of deep convection and sea–ice feedbacks on the background state.

In a weakly forced scenario, such as the solar minimum scenario employed in this work, dynamical feedbacks involving diabatically forced stationary waves and sea–ice in the North Pacific play a crucial role in determining the regional-scale response. Consequently, these processes are key to understand the uncertainty in regional-scale climate change projections in the NH.

As the role of future solar activity is underrepresented in the design of simulations participating in IPCC assessment reports (Kirtman *et al* 2013, Myhre *et al* 2013, Ineson *et al* 2015), we conclude that it needs to be taken into account by designing solar forcing scenarios such as those performed in this study. Due to inter-model differences in the parameterizations of tropical convection, sea–ice, and their interaction with the general circulation, the impact of a solar minimum scenario is likely to be model dependent. Nonetheless, insights can be gained into the sensitivity of regional-scale projections and the involved processes, which are crucial towards an improved characterization of the inter-model spread in climate projections.

Acknowledgments

We thank the editor for handling this paper and the anonymous reviewers for their constructive feedback. We also gratefully acknowledge Isla Simpson and Minfang Ting for providing the stationary wave model code. This research has been supported by the Supercomputing Centre of Galicia (CESGA) through three ICTS projects and FEDER funds. In addition, computing resources were also provided by the Barcelona Supercomputing Center through three RES activities, and by the EOLO cluster of excellence at Universidad Complutense de Madrid. G Chiodo was partly supported by the Spanish Ministry of Education in the framework of the FPU doctoral fellowship (grant AP2009-0064). This work was supported by the Spanish Ministry of Science and Innovation (MCINN) through the CONSOLIDER (CSD2007-00050-II-PR4/07), MATRES (CGL2012-34221), and ExCirEs (CGL2011-24826) projects, and by the European Commission within the FP7 framework through the StratoClim project (Ref. 603557). JM Vaquero acknowledges the support from the Junta de Extremadura (Research Group Grants GR10131) and from the Spanish Government (AYA2011-25945 and AYA2014-57556-P). The authors also aknowledge the COST Action ES1005 TOSCA (http://tosca-cost.eu) and the WCRP/SPARC SOLARIS-HEPPA project (http://solarisheppa.geomar.de/).

References

Abreu J, Beer J, Steinhilber F, Tobias S and Weiss N 2008 For how long will the current grand maximum of solar activity persist? *Geophys. Res. Lett.* **35** L20109

Anet J *et al* 2013 Impact of a potential 21st century grand solar minimum on surface temperatures and stratospheric ozone *Geophys. Res. Lett.* **40** 4420–5

Bader J, Mesquita M D, Hodges K I, Keenlyside N, Østerhus S and Miles M 2011 A review on northern hemisphere sea–ice, storminess and the north atlantic oscillation: observations and projected changes *Atmos. Res.* **101** 809–34

Deser C, Phillips A, Bourdette V and Teng H 2012 Uncertainty in climate change projections: the role of internal variability *Clim. Dyn.* **38** 527–46

Ermolli I *et al* 2013 Recent variability of the solar spectral irradiance and its impact on climate modelling *Atmos. Chem. Phys.* **13** 3945–77

Feulner G and Rahmstorf S 2010 On the effect of a new grand minimum of solar activity on the future climate on Earth *Geophys. Res. Lett.* **37** L05707

Gray L *et al* 2010 Solar influences on climate *Rev. Geophys.* **48** RG4001
Haigh J, Blackburn M and Day R 2005 The response of tropospheric circulation to perturbations in lower-stratospheric temperature *J. Clim.* **18** 3672–85
Haigh J D 1996 The impact of solar variability on climate *Science* **272** 981–4
Harnik N, Seager R, Naik N, Cane M and Ting M 2010 The role of linear wave refraction in the transient eddy-mean flow response to tropical pacific sst anomalies *Q. J. R. Met. Soc.* **136** 2132–46
Hartmann D L 1994 *Global Physical Climatology* 56 (New York: Academic)
Held I M, Ting M and Wang H 2002 Northern winter stationary waves: theory and modeling *J. Clim.* **15** 2125–44
Holland M M and Bitz C M 2003 Polar amplification of climate change in coupled models *Clim. Dyn.* **21** 221–32
Hoskins B J and Ambrizzi T 1993 Rossby wave propagation on a realistic longitudinally varying flow *J. Atmos. Sci.* **50** 1661–71
Ineson S *et al* 2015 Regional climate impacts of a possible future grand solar minimum *Nat. Commun.* **6** 7535
Janardhan P, Bisoi S K, Ananthakrishnan S, Tokumaru M and Fujiki K 2011 The prelude to the deep minimum between solar cycles 23 and 24: interplanetary scintillation signatures in the inner heliosphere *Geophys. Res. Lett.* **38** L20108
Jin F and Hoskins B J 1995 The direct response to tropical heating in a baroclinic atmosphere *J. Atmos. Sci.* **52** 307–19
Jones G S, Lockwood M and Stott P A 2012 What influence will future solar activity changes over the 21st century have on projected global near-surface temperature changes? *J. Geophys. Res.* **117** D05103
Kinnison D *et al* 2007 Sensitivity of chemical tracers to meteorological parameters in the MOZART-3 chemical transport model *J. Geophys. Res.* **112** D20302
Kirtman B *et al* 2013 Near-term climate change: projections and predictability *Climate Change 2013: The Physical Science Basis. Contribution of Working Group I to the Fifth Assessment Report of the Intergovernmental Panel on Climate Change* ed T Stocker *et al* (New York: Cambridge University Press)
Kodera K and Kuroda Y 2002 Dynamical response to the solar cycle *J. Geophys. Res.* **107** 4749
Kushnir Y, Seager R, Ting M, Naik N and Nakamura J 2010 Mechanisms of tropical atlantic sst influence on north American precipitation variability *J. Clim.* **23** 5610–28
Lean J 2000 Evolution of the Sun s spectral irradiance since the maunder minimum *Geophys. Res. Lett.* **27** 2425–8
Lean J, Rottman G, Harder J and Kopp G 2005 Sorce contributions to new understanding of global change and solar variability *Solar Rad. Clim. Exp.* (*SORCE*) 27–53
Lockwood M 2011 Was uv spectral solar irradiance lower during the recent low sunspot minimum? *J. Geophys. Res.* **116** D16103
Lockwood M, Owens M, Barnard L, Davis C and Steinhilber F 2011 The persistence of solar activity indicators and the descent of the sun into maunder minimum conditions *Geophys. Res. Lett.* **38** L22105
Mantua N J, Hare S R, Zhang Y, Wallace J M and Francis R C 1997 A pacific interdecadal climate oscillation with impacts on salmon production *Bull. Am. Met. Soc.* **78** 1069–79
Marsh D R, Mills M J, Kinnison D E, Lamarque J-F, Calvo N and Polvani L M 2013 Climate change from 1850 to 2005 simulated in CESM1 (WACCM) *J. Clim.* **26** 7372–91
Matthes K, Kuroda Y, Kodera K and L U 2006 Transfer of the solar signal from the stratosphere to the troposphere: northern winter *J. Geophys. Res.* **111** D06108
Maycock A *et al* 2015 Possible impacts of a future grand solar minimum on climate: stratospheric and global circulation changes *J. Geophys. Res.* **120** 9043–58
McCracken K and Beer J 2014 Comparison of the extended solar minimum of 2006–2009 with the spoerer, maunder, and dalton grand minima in solar activity in the past *J. Geophys. Res.* **119** 2379–87
Meehl G, Arblaster J, Matthes K, Sassi F and van Loon H 2009 Amplifying the Pacific climate system response to a small 11 year solar cycle forcing *Science* **325** 1114–8
Meehl G A and Arblaster J M 2009 A lagged warm event-like response to peaks in solar forcing in the pacific region *J. Clim.* **22** 3647–60
Meehl G A, Arblaster J M and Marsh D R 2013 Could a future grand solar minimum like the maunder minimum stop global warming? *Geophys. Res. Lett.* **40** 1789–93
Meehl G A, Washington W M, Wigley T, Arblaster J M and Dai A 2003 Solar and greenhouse gas forcing and climate response in the twentieth century *J. Clim.* **16** 426–44
Myhre G *et al* 2013 Anthropogenic and natural radiative forcing *Climate Change 2013: The Physical Science Basis. Contribution of Working Group I to the Fifth Assessment Report 576 of the Intergovernmental Panel on Climate Change* ed T Stocker *et al* (Cambridge: Cambridge University Press)
Nandy D, Munoz-Jaramillo A and Martens P C 2011 The unusual minimum of sunspot cycle 23 caused by meridional plasma flow variations *Nature* **471** 80–2
Overland J E and Wang M 2010 Large-scale atmospheric circulation changes are associated with the recent loss of arctic sea ice *Tellus* A **62** 1–9
Roth R and Joos F 2013 A reconstruction of radiocarbon production and total solar irradiance from the holocene 14 c and co 2 records: implications of data and model uncertainties *Clim. Past* **9** 1879–909
Roy I and Haigh J D 2010 Solar cycle signals in sea level pressure and sea surface temperature *Atmos. Chem. Phys.* **10** 3147–53
Schaller N, Sedlacek J and Knutti R 2014 The asymmetry of the climate system response to solar forcing changes and its implications for geoengineering scenarios *J. Geophys. Res.* **119** 5171–84
Schrijver C, Livingston W, Woods T and Mewaldt R 2011 The minimal solar activity in 2008–2009 and its implications for long-term climate modeling *Geophys. Res. Lett.* **38** L06701
Seager R, Naik N, Ting M, Cane M, Harnik N and Kushnir Y 2010 Adjustment of the atmospheric circulation to tropical pacific sst anomalies: variability of transient eddy propagation in the pacific-north america sector *Q. J. R. Met. Soc.* **136** 277–96
Serreze M, Barrett A, Stroeve J, Kindig D and Holland M 2009 The emergence of surface-based arctic amplification *Cryosphere* **3** 11–9
Serreze M C and Barry R G 2011 Processes and impacts of arctic amplification: a research synthesis *Glob. Plan. Change* **77** 85–96
Shapiro A, Schmutz W, Rozanov E, Schoell M, Haberreiter M, Shapiro A and Nyeki S 2011 A new approach to the long-term reconstruction of the solar irradiance leads to large historical solar forcing *Astron. Astrophys.* **529** A67
Shindell D, Rind D, Balachandran N, Lean J and Lonergan P 1999 Solar cycle variability, ozone, and climate *Science* **284** 305–8
Simmons A 1982 The forcing of stationary wave motion by tropical diabatic heating *Q. J. R. Met. Soc.* **108** 503–34
Simpson I R, Blackburn M and Haigh J D 2009 The role of eddies in driving the tropospheric response to stratospheric heating perturbations *J. Atmos. Sci.* **66** 1347–65
Simpson I R, Seager R, Ting M and Shaw T A 2015 Causes of change in northern hemisphere winter meridional winds and regional hydroclimate *Nat. Clim. Change* **2783**
Solanki S and Fligge M 1999 A reconstruction of total solar irradiance since 1700 *Geophys. Res. Lett.* **26** 2465–8
Song X, Lubin D and Zhang G J 2010 Increased greenhouse gases enhance regional climate response to a maunder minimum *Geophys. Res. Lett.* **37** L01703
Thompson D and Wallace J 1998 The arctic oscillation signature in the wintertime geopotential height and temperature fields *Geophys. Res. Lett.* **25** 1297–300
Ting M and Yu L 1998 Steady response to tropical heating in wavy linear and nonlinear baroclinic models *J. Atmos. Sci.* **55** 3565–82
Usoskin I G *et al* 2015 The maunder minimum (1645–1715) was indeed a grand minimum: a reassessment of multiple datasets *Astron. Astrophys.* **581** A95

van Loon H and Meehl G A 2014 Interactions between externally forced climate signals from sunspot peaks and the internally generated pacific decadal and north atlantic oscillations *Geophys. Res. Lett.* **41** 161–6

van Loon H, Meehl G A and Shea D J 2007 Coupled air–sea response to solar forcing in the pacific region during northern winter *J. Geophys. Res.* **112** D02108

Zhang C 1993 Large-scale variability of atmospheric deep convection in relation to sea surface temperature in the tropics *J. Clim.* **6** 1898–913

Zolotova N V and Ponyavin D I 2014 Is the new Grand minimum in progress? *J. Geophys. Res.* **119** 3281–5

Zwiers F W and von Storch H 1995 Taking serial correlation into account in tests of the mean *J. Clim.* **8** 336–51